EUROPEAN ORGANIZATION FOR NUCLEAR RESEARCH

CERN-ISRC/79-11
ISR/P 102
9 April 1979

PROPOSAL

PRECISE MEASUREMENT OF THE PROTON-ANTIPROTON TOTAL CROSS-SECTION AT THE CERN ISR

CERN[1]-MIT[2]-Pisa[3]-Stony Brook[4] Collaboration

U. Becker[1], G. Carboni[3], V. Cavasinni[3*], T. Del Prete[3*],
G. Finocchiaro[4], P. Grannis[4], M. Morganti[3], D. Lloyd-Owen[4],
J. Paradiso[2] and M. Valdata-Nappi[3]

G E N E V A
1979

1) CERN, Geneva, Switzerland.

2) MIT, Massachusetts Institute of Technology, Cambridge, MA, USA.

3) Sezione I.N.F.N. and Istituto di Fisica dell'Università, Scuola Normale Superiore, Pisa, Italy.

4) State University - Stony Brook, N.Y., USA.

*) CERN Fellow.

1. INTRODUCTION

The first fundamental quantity that has to be measured in order to study strong interactions is the total cross-section. In the case of proton-proton collision, it was for a long time believed that this cross-section $[\sigma(pp)]$ was constant as a function of energy. One of the big achievements of the CERN ISR was to demonstrate[1] that this cross-section is rising at very high energy. Measurements at FNAL[2] confirmed this to be a general property of most strong interaction total cross-sections (Fig. 1). But for the antiproton-proton total cross-section measurements $[\sigma(\bar{p}p)]$, even at the highest FNAL energies, the rise of $\sigma(\bar{p}p)$ has not yet been observed. In any case, dispersion relation arguments[3] and the observation that there are more reaction channels open for $\bar{p}p$ than for pp interactions suggest that $\sigma(\bar{p}p)$ will lie above $\sigma(pp)$, therefore rising by at least 1.5 mb over the full ISR energy range (Fig. 1). Thus the increase would start at ISR energies and should be large enough to be measurable.

The difference $\Delta\sigma$ between $\sigma(\bar{p}p)$ and $\sigma(pp)$ shows the strikingly simple pattern of behaviour seen in Fig. 2. The difference $\Delta\sigma$ is well parametrized with a power law in laboratory momentum[4],

$$\Delta\sigma \propto p_{lab}^{-0.61} ,$$

and is expected to range between 2.0 and 0.6 mb over the ISR energy range. Figure 2 contains also low-energy annihilation data. While the identification of $\Delta\sigma$ with a measurement of annihilation processes is a much debated question[4], the study of the difference also in terms of topological cross-sections and correlation functions (together with their energy dependence) is undoubtedly an interesting piece of physics, offering a possible tool for investigating the physical nature of the process responsible for $\Delta\sigma$. Theoretically, the main advantage in studying the differences is that the contribution of the amplitudes that are odd under cross-channel charge conjugation can be isolated. In the simple Regge-Mueller picture, that complicated object called the Pomeron is, in particular, absent, thus enhancing the predictive power of the model.

We propose to measure $\sigma(\bar{p}p)$ at the five ISR energies, $\sqrt{s}$ = 23.5 GeV to $\sqrt{s}$ = 62.7 GeV. The measurement of $\sigma(pp)$ will also be performed under similar running conditions in order to have a minimum biased study of $\Delta\sigma$.

The expected small relative increase of $\sigma(\bar{p}p)$ (1.5 mb) and the limited difference $\Delta\sigma$ (2.0 to 0.6 mb) imply that the total cross-section measurement has to be done with high precision, i.e. a relative error $\Delta\sigma/\sigma \lesssim 1\%$.

The unique feature offered by the ISR, i.e. a direct comparison of $\bar{p}p$ and pp interactions using the same apparatus, will allow us to minimize several experimental biases. Moreover in recent years the ISR have improved their operation, not only by reaching the highest luminosities but also by handling background problems efficiently, even in low-intensity runs. Today, the reliability of the machine gives a good guarantee of the quality of $\bar{p}p$ operations; and on this we will base most of our further discussions.

We propose to exploit the same methods as that used for the first time at the ISR by the Pisa-Stony Brook (PSB) Collaboration in intersection region I 8 [1]. Since this proposed experiment is an improvement on the previous PSB one, using also a good deal of the already existing equipment (now installed and operational in I 2), we shall concentrate our attention mainly on the applicability of the method to the $\bar{p}p$ case and on the improvements we may get at present. Many data, especially those for an estimate of randoms, extrapolations, and corrections necessary for the determination of the total cross-section, will be taken from the previous experiment on pp.

The original PSB set-up, based on large scintillation counter hodoscopes, has been upgraded in experiment R209 with a drift chamber system covering almost the full solid angle[5]. This extension will be essential for reducing many systematic errors on the total cross-section measurement.

The chamber system together with the largely inclusive triggering capability of the hodoscopes will allow us to do a more precise measurement of the topoligical cross-sections at multiplicity n, $\sigma^n(pp)$ and $\sigma^n(\bar{p}p)$, and of the several correlation functions[6].

2. EXPERIMENTAL METHOD

The total cross-section is defined by

$$\sigma(\bar{p}p) = \frac{R_{tot}}{L_{ISR}} ,$$

where R_{tot} is the total interaction rate and L_{ISR} is the is the ISR luminosity; L_{ISR} will be measured by the Van der Meer method (VDM)[7], by displacing the two beams vertically in precise steps. If $R_M(\delta)$ is the rate of a monitor M, as a function of the relative beam displacement δ, then

$$\int_{-\infty}^{+\infty} R_M(\delta)\, d\delta = \frac{\sigma_M}{K} I_1 I_2 , \qquad (1)$$

where

I_1, I_2 are the beam currents,

α is the beam intersecting angle,

$$K = \beta c e^2 \frac{\sin \alpha/2}{\left[1 - \beta^2 \sin^2(\alpha/2)\right]^{\frac{1}{2}}} \simeq \beta \times 0.9972 \times 10^{-28} \ (A^2 \text{ cm sec}) ,$$

σ_M is the fraction of cross-section seen by the monitor.

The luminosity is then measured by

$$L = R_M/\sigma_M .$$

The total cross-section is thus obtained by scaling σ_M with the ratio of the total rate to measured rate.

The total hadronic interaction rate can only be measured in part, because of the incomplete coverage of the solid angle of our scintillation counter system. Thus

$$R_{tot} = R_{meas} \left(1 + \varepsilon + \eta^{inel}_{extr} + \eta^{el}_{extr}\right) , \qquad (2)$$

where R_{meas} is the measured rate; ε accounts for inefficiencies due to dead spaces between counters and accidental losses; η^{el}_{extr} accounts for those elastic scattering events which, at such a small angle, remain in the beam vacuum pipe; η^{in}_{extr} accounts for inelastic events lost by the trigger because of incomplete geometrical coverage (mostly at small angle).

3. EXPERIMENTAL SET-UP

A sketch of the experimental apparatus is shown in Fig. 3. The detector is symmetric with respect to the interaction point and consists of

- scintillation counter hodoscopes,
- a drift chamber central detector.

3.1 Scintillation counter system

The scintillation counter system is essentially the same as that used in the PSB experiment[1], now installed and running in I 2 (experiment R 209).

Each arm of the apparatus consists of hodoscopes H1, H2, H3, H4, and TB. The azimuthal coverage downstream from each beam is complete. Hodoscopes H1 and H2, 2 m away from the beam crossing point, detect particles produced at angles $4^\circ \lesssim \theta \lesssim 33^\circ$. In a similar way, hodoscopes H3 and H4, at 6.4 and 7.7 m from the crossing point respectively, cover a θ interval between $\simeq 0.8^\circ$ and $\simeq 6.7^\circ$. Each

arm is completed by small hodoscopes (TB) positioned downstream from hodoscope H4, in the region where the thin circular vacuum pipe has narrowed to an elliptical cross-section. They allow detection of particles emitted at angles as small as 0.3°. These counters are used to recover an important fraction of elastically or quasi-elastically scattered particles.

A large-angle detector (CI, CO hodoscopes) surrounds the interaction region and covers the region at angles larger than 25° with respect to either beam over the full azimuthal angle.

Dimensions, positions, and angles subtented by each hodoscope are given in Tables 1 and 2. The geometries of the hodoscopes are sketched in Fig. 4.

In order to have a rough measure of the emission angles of the particles produced in each cone, two additional hodoscopes H2θ and H4θ are placed behind H2 and H4. Hodoscopes H2θ and H4θ split the polar angle θ into 9 and 14 regions, respectively (see Fig. 5). Dimensions and angles subtented by each counter are given in Table 3.

In a similar way the TB counters are supplemented by an x, y array of scintillation counters finely divided into strips 2 cm wide (Fig. 5). A measurement of angular distribution in this region is important for extrapolating the elastic and inelastic events lost in the beam-pipe hole (see Section 4).

3.2 Drift chamber central detector

The drift chamber detector that we plan to use is the same as that now in operation in experiment R 209. It consists of 136 modules held together in plexiglas containers, covering the full azimuth and down to 7° in polar angle along each beam. The details of this system have already been published[8]. A view of the whole system is shown in Fig. 6. Each module contains two doublets of sense wires, each doublet facing one delay line so as to determine the space points directly, without left-right ambiguities. The space resolution is $\sim \pm 0.2$ mm in the drift coordinate (polar angle) and $\sim \pm 2.0$ mm in the delay-line coordinate (azimuthal angle). This system has proved to be quite realiable in pattern recognition efficiency and operation.

3.3 Trigger logic

The basic trigger requires at least one charged particle in both the left and right arm of the apparatus or in one arm and in the central hodoscopes CI, CO, which we can write:

$$T = [H3*H4 + H1*H2 + TB]_{left} * [H3*H4 + H1*H2 + CI*CO + TB]_{right} .$$

The CI, CO hodoscopes are conventionally attributed to the right side.

Whenever T occurs, the timing of signals coming from the counters is digitized and recorded together with the real time of the experiment, the pattern of the hit counters, and the chamber drift times.

The resolving time of the main trigger T is kept rather wide in order to accept an appreciable amount of background events. The time-of-flight (TOF) distribution of pairs of hodoscopes is shown in Fig. 7 (taken from the previous PSB experiment). An accurate off-line analysis of these distributions will allow the precise counting of beam-beam events; details of this analysis will follow the same pattern as in proton-proton case and can be found in Ref. 1. The main error in the counting of beam-beam events is of a systematic nature because of single beam subtraction. In the PSB experiment the error was estimated to be $\sim 0.3\%$, independent of the ISR energy. The loss of luminosity due to the lower $\bar{p}$ beam intensity (a factor of ~ 10 less than in the PSB experiment) is largely redeemed, with respect to the signal-to-background ratio, by a better quality of vacuum inside the beam pipes (now 10^{-13} Torr) and the better general ISR operations, so that the determination of R_{meas} is expected to have negligible systematic error ($\lesssim 0.1\%$) both for $\bar{p}p$ and pp reactions. Dead-time losses and random effects, included in the factor ε in formula (2), can be continously monitored using light-emitting diodes (LED) attached to each counter which can simulate real events[5]. Moreover, dead-space losses, important only in low multiplicity events, can be measured in special runs in which the trigger is modified by changing the logical AND of facing hodoscope planes into logical OR (i.e. H3*H4 into H3+H4). In the PSB experiment, ε was found to be 0.012 ± 0.002 and there is no reason why this correction should not be the same in the $\bar{p}p$ interaction.

It is important to realize that, using this procedure, the measurement of the total rate has the following advantages:

- it has proved to handle all beam conditions well, even very bad ones;
- its permits a fast and relatively simple analysis of the data, using a minimum amount of computer time;
- it is highly inclusive (see Table 4 showing the fraction R_{meas}/R_{tot} that can be seen at each energy, and the relative contribution of each TOF in the proton-proton case).

3.4 Trigger extensions

The trigger described in the previous section has proved to be powerful in the pp reaction. However, a major difference exists between the $\bar{p}p$ and pp reactions; the total charge of final states is zero in $\bar{p}p$ but two in pp. This might imply larger trigger losses. Measurements at FNAL[4,9] show that topological cross-sections (Fig. 8) are different mainly in the zero-prong channel (which cannot exist in pp reactions). This channel is expected to be negligible at ISR energies

($\lesssim$ 10 μb, from the dashed curve in Fig. 8). Moreover, at FNAL energies the inclusive single-particle distributions in $\bar{p}p$ and pp reactions are rather similar, leading to the conclusion that there is no evidence that the trigger will be less in-inclusive in the $\bar{p}p$ case than in the pp one.

To additionally check unlikely topologies, we consider the following extensions:

i) Insertion of lead converters in front of the main hodoscopes during special runs. In this way the system will became more inclusive, detecting also π^0's.

ii) The use of a "one-arm trigger left *OR* right" in special runs. In this case the rejection of the background becomes a major problem because the TOF system no longer helps, and the tracking of charged particles and vertex reconstruction with our drift chamber system will therefore become necessary. This method has figures of merit complementary to the left-right trigger:

- reduction of inelastic extrapolation corrections (the rescuing of a large fraction of single diffractive events);
- more safety in inelastic events recognition. It is possible to imagine events, never firing a left-right trigger (annihilation with charged particles in one hemisphere only, or only jets at $\sim 90°$), that cannot be rescued by extrapolation techniques.

4. CORRECTIONS

4.1 Elastic losses

The minimum triggering angle (θ_{min}) is fixed by the holes in hodoscope system to accommodate beam exit pipes. Since the elastic differential cross-section in this region of momentum transfer t is well parametrized by $d\sigma/dt \propto e^{-b|t|}$, it is clear that elastic losses depend on energy. To first approximation the losses would be

$$\sigma^{el}_{lost} \simeq b\sigma^{el}(\theta_{min}\, p_{ISR})^2 \ .$$

This formula shows the geometrical nature of the extrapolation, its energy dependence being dominated by the p^2_{ISR} factor. In the case of the pp reaction, the $\sigma^{el} \times b$ term varies by $\sim$ 20% over ISR energies (see Table 5), while the p^2_{ISR} accounts for a factor of $\sim$ 10.

The available data on b and σ_{el} are shown in Fig. 9 for pp and $\bar{p}p$ reactions[10]. The values of the slope for $\bar{p}p$ are approaching the pp ones from above and should be almost equal at ISR energies. Also at PS energies the integrated cross-section has nearly the same value in both cases and seems to have the same energy dependence.

The way in which we can compute elastic extrapolation losses is twofold:

i) extrapolate the differential cross-section, as seen by our apparatus, to 0°;

ii) integrate the $\bar{p}p$ elastic cross-section, as measured by other groups at the ISR or as inferred from lower-energy data, over the solid angle left uncovered because of beam pipes.

The first method requires a study of angular distributions at small angles. This is achieved with the finely divided TB hodoscope covering angles down to 5 mrad (see Fig. 5 and Table 2). Some corrections have to be applied to the angular distribution because of interactions between elastically scattered particles and the beam pipe. The amount of this effect was calculated in PSB geometry, showing that $\sim$ 20% of elastic events had an interaction and could not be tagged as elastic. A detailed calculation of the corrections and their errors depends on the exact geometry and has not yet been performed. It seems anyway quite conservative to assume $\Delta b/b \sim \pm 10\%$ and $\Delta\sigma^{el}/\sigma^{el} \sim \pm 5\%$ as measured from our distribution. Table 5 shows the expected extrapolations and their errors. This error will of course be considerably reduced as soon as dedicated experiments can clarify the $\bar{p}p$ elastic scattering process at ISR energies.

4.2 Inelastic losses

The left-right trigger loses those events having particles in one hemisphere below the minimum triggering angle (single diffractive events). Again, the amount of loss can be estimated from the results of the PSB experiment. Here the recovery was performed by measuring the distribution of the maximum polar angle for each event and extrapolating it to 0° [1]. Table 6 shows what the correction was as a function of p_{ISR}. It should be noted that the use of a "one arm only" trigger would make this correction negligible.

5. MEASUREMENT OF THE ISR LUMINOSITY

As we have anticipated, the luminosity will be measured by the Van der Meer (VDM) method[7]. As in the PSB experiment, we shall use part of our hodoscope system as the monitor; for instance

$$M = (H3*H4)_{left}*(H3*H4)_{right} .$$

The important advantages of this monitor are:

- a large detected cross-section $\sigma_M > 1/2\ \sigma_{tot}$;
- high stability over months of running time;
- it is independent of beam stacks (radial position of beams);

- good handling of background by TOF chains;
- reliable corrections (randoms, losses, etc.).

This method provided results with a relative error of $\lesssim \pm 0.5\%$, but with a scale error that could not be reduced below 1.0% [11]. These errors were mainly caused by rounding off errors in the current setting of magnets responsible for beam vertical bumps, by residual hysteresis effect, and, in general, by an incomplete understanding of the details of the ISR optics.

The most important improvement which is necessary if we want to gain in precision with respect to the previous PSB experiment, is to reduce the error on luminosity calibration. This is possible because

i) understanding of systematic effects, such as magnetic hysteresis, has been achieved by the use of precise scrapers in I 5 and I 7 [12];

ii) the background has decreased by a factor of $\sim$ 10 owing to improved ISR operations. This is a general benefit, in particular for the tails of the VDM calibration curve;

iii) we propose to equip our intersection region with the precise magnetic beam position detectors[13] $\sim$ 3 m upstream of the crossing point. These devices give a direct measurement of beam centroids with errors of ± 10 μm and negligible scale error. They have been designed to work with currents of $\sim$ 5 A, but they can easily be adjusted to keep the same precision with the expected $\bar{p}$ intensities of $\sim$ 150 mA [14].

In this way we have eliminated the scale error and reduced the point-to-point errors. The error on the luminosity integral now depends on counting rate statistics and on the ratio of uncertainties in beam position (Δz) to the dispersion of luminosity curve. Quantitatively speaking, if we count for a fixed time at each point of the curve, the statistical errors can be expressed by

$$\frac{\Delta\sigma_M}{\sigma_M} = \frac{1}{\sqrt{N_{tot}}} ,$$

N_{tot} being the total number of events collected in the measurement. To get a relative error of $\pm 0.1\%$ the measurement would last $\sim$ 2 hours, with the optimized beams for luminosity measurements ($L \sim 10^{28}$ cm^{-2} sec^{-1}).

The dependence of relative error on vertical beam displacement uncertainties can be computed. In the case of a Gaussian-shaped luminosity curve with dispersion Σ, we find

$$\frac{\Delta\sigma_M}{\sigma_M} = \frac{1}{2\sqrt[4]{\pi}} \frac{\Delta z}{\Sigma} \sqrt{\frac{\Delta\delta}{\Sigma}} ,$$

where $\Delta\delta$ are the steps by which the curve is scanned. With standard values of Z and $\Delta\delta$ the calculation gives

$$\frac{\Delta\sigma_M}{\sigma_M} < 0.1\% \ .$$

The monitor cross-section can therefore be safely measured with relative error $\lesssim 0.2\%$, the ultimate answer coming from the reproducibility of measurements over different running conditions.

6. PRECISION OF THE ($\bar{p}p$) MEASUREMENT

From all the previous discussions, we have tried to clarify the several factors which contribute to $\sigma(\bar{p}p)$ and how well they could be measured. Table 7 summarizes all the errors affecting the value of $\sigma(\bar{p}p)$, showing that the precision attainable should be almost as high as the one from transmission methods at fixed-target accelerators. This fact also represents progress in the measurement of the pp reaction.

7. INSTALLATION

7.1 Intersection region

In order to explore the small-angle region, we need to have the experiment installed in an even-numbered ISR crossing point, preferably I 2. In fact in this interaction region most of the equipment is already installed and cabled. Only three hodoscope planes need to be rebuilt: H1 (right and left) and H2 (right). The small-angle x,y array set behind the TB counters is a completely new small hodoscope, and it must be designed and built. H2θ (right) and TB counters must be installed.

The hodoscopes H3, H4 and H4θ on the left and right arm, the CI, CO counters, H2 and H2θ on the left arm, and the drift chamber detector are mounted on experiment R 209.

7.2 Experiment timetable

On the assumption that we can continue to use the equipment at present installed in I 2, and based on the expected ISR timetable, we plan to install the missing hodoscopes in January 1980.

During 1980 we shall remeasure σ(pp) to check the performances of the apparatus and, in particular, to get the beam displacement monitors operational.

In the same year we foresee applying the same method to proton-deuteron and deuteron-deuteron reactions. The details of these extensions will be given in a separate paper.

Physics with antiprotons will be performed partly during 1981 and mainly in 1982.

7.3 Running

Special runs will be needed for luminosity calibration in clean ISR beam conditions. Since the experiment is a high-rate one, we have in fact to optimize for background rather than for absolute luminosity. Of course the best over-all running conditions will be found empirically.

We will also need to alternate runs for $\bar{p}p$ and pp under similar conditions in order to reduce all possible distortions in the comparison between the two cross-sections. Also, the five standard ISR energies ($\sqrt{s}$ = 23, 31, 44, 53, 63 GeV) will be needed so as to have the complete picture of energy dependence.

The Terwilliger scheme could be necessary to reduce the diamond spot in the special runs with a "single arm" trigger.

Special runs with only one beam circulating in the machine will be needed for the study of single-beam background.

8. PHYSICS PROGRAMME EXTENSIONS

This apparatus is able to measure $\sigma(\bar{p}p)$ and $\sigma(pp)$ with high precision. It is also equipped with devices that allow a more detailed study of the properties of these interactions. The drift chamber detector and the finely divided counter system measure the final-state charge multiplicity and angular distributions. This also opens up the field of inclusive physics, i.e.

- multiplicity distributions and their moments,
- single-particle distributions (inclusive, at fixed multiplicity etc),
- correlation functions etc.

The scintillation counter system and the drift chamber system offer a complementary way to study these processes. The former is in fact capable of handling and processing a very high number of events but with low precision (binning effects, secondary interactions). The latter is very much better for anything concerning spatial resolution and background track rejection, but is capable of handling only limited statistics.

A particularly important channel that can be studied is the elastic scattering at relatively small momentum transfer, i.e. $|t| \lesssim 0.5$ $(GeV/c)^2$, to explore the difference in the shape of $\bar{p}p$ and pp reactions (cross-over effect). These events could be tagged by requiring only two collinear tracks with the correct TOF pattern.

This apparatus can be used to study several reactions. Proton-proton and proton-antiproton reactions can be studied with the aforesaid precision. A similar study of proton-deuteron and antiproton-deuteron can also be pursued, hopefully by tagging the reaction proton-neutron with the detection of the spectator proton swept

away in the ISR bending magnet. The evaluation of the efficiency of this method and the attainable precision will be discussed in a further document.

We would also like to point out that the investigation of antiproton-antiproton reactions will become possible at the ISR, an option never before available. This could be performed at lower energy, filling Ring 1 with one bunch of 3.5 GeV/c antiprotons coming directly from the antiproton accumulator via the TT2 beam transfer tunnel. This bunch could be accelerated up to the ISR transition energy (8.5 GeV), and eventually even above it if the critical energy could be passed. The other ring could be filled in the standard way. The ISR luminosity would be $L \sim 10^{26}$ (cm^{-2} sec^{-1}) and the total rate $\sim$ 4 events/sec. It is important to note that all this does not imply any construction of tunnels etc.; it uses only the existing facility of sending antiprotons in either direction in TT2 [15].

The physics that our detector could explore in antiproton-antiproton stacks includes:

- $\sigma(\bar{p}\bar{p})$. No surprise is expected since $\sigma(\bar{p}\bar{p}) = \sigma(pp)$ via CPT invariance. The relative error of the measurement would be $\Delta\sigma/\sigma \sim 1\%$ if we have no problem with the background.
- Single-particle distributions, correlations, etc., are connected to the pp reaction via C-invariance alone. A direct comparison of these distributions could provide a test of the C-invariance at these energies in strong interactions, which should be good down to a fraction of a percent.
- Completely unexpected features of $\bar{p}\bar{p}$ interactions that are different from those of the pp case.

9. CONCLUSIONS

Most of the experimental set-up described in this proposal is at present installed and operational in I 2. The main efforts that will be needed to modify the present set-up to suit the proposed experiment are:

i) to build H1 (left and right) using a new design;

ii) to build the small TB array hodoscopes (left and right);

iii) to build H2 right;

iv) to install all the above counters as well as H2θ right.

We have made this planning having in mind that the equipment which is now operational in I 2 will remain at the ISR to be used for the proposed experiment. This equipment is

- the hodoscope system H3, H4, H4θ (letf and right), H2 left, H2θ left, CI, CO, and the drift chamber detector;

- the electronics connected to it, mainly:

  a) fast NIM logic,

  b) drift chamber read-out system,

  c) CAMAC and data acquisition system, including the HP on-line computer.

  We would need the following help from CERN:

  a) The necessary stands to hold in place the drift chamber system and CI, CO counters, at present incorporated into the μ-spectrometer.

  b) Stands for the new H2, H2θ hodoscopes.

As a matter of fact part of the R 209 equipment is also of interest for the UA4 Collider experiment. Discussions are going on with that group regarding a possible sharing of the apparatus. However, if an essential part of the apparatus is eventually removed from I 2, we would also ask CERN to cover the effort needed to replace it.

Computer time requests are limited to:

- fast turn-around checks on the experimental set-up;
- analysis of the TOF spectra in order to control the efficiency, background, measurements of the ISR luminosity, etc.

This leads us to estimate that $\sim$ 20 CPU 7600 equivalent hours per year will be sufficient. The most time-consuming job of tracking charged particles using the drift chamber detector is in fact planned to be done in our home institutes.

The participation of the various laboratories involved is subject to the approval of each home institute.

REFERENCES

1) U. Amaldi et al., Phys. Letters 44B, 112 (1973).
S.R. Amendolia et al., Phys. Lett. 44B, 119 (1973).
2) S.R. Amendolia et al., Nuovo Cimento 17A, 735 (1973).
CERN-Rome-Pisa-Stony Brook Collab., Phys. Lett. 62B, 460 (1976).
U. Amaldi et al., Nucl. Phys. B145, 367 (1978).

2) A.S. Carroll et al., Phys. Rev. Lett. 33, 928 (1974).
A.S. Carroll et al., Phys. Rev. Lett. 33, 932 (1974).
A.S. Carroll et al., Phys. Lett. 61B, 303 (1976).
A.S. Carroll et al., Phys. Lett. 80B, 423 (1979).

3) U. Amaldi et al., Phys. Lett. 66B, 390 (1977).

4) A compilation of data can be found in J.C. Rushbrooke and B-R. Webber, Phys. Reports 44, 1 (1978). Data from Ref. 2 have also been used.

5) S.R. Amendolia et al., Large coverage counter system of the total pp cross-section experiment at the ISR, Int. Conf. on Instrumentation for High-Energy Physics, Frascati, 1973, CNEN, Frascati, 1973, p. 391.

6) G. Bellettini et al., Phys. Lett. 45B, 69 (1973).
S.R. Amendolia et al., Phys. Lett. 48B, 359 (1974).
S.R. Amendolia et al., Nuovo Cimento 61, 17 (1976).

7) Van der Meer, CERN Internal Report ISR-PO/68-31)1968).

8) A. Bechini et al., Nucl. Instrum. Methods 156, 181 (1978).

9) A compilation of data can be found in J. Whitmore, Phys. Reports 27C (1976); J.C. Rusnbrooke et al., Phys. Lett. 59B, 303 (1975).

10) We have followed the compilation of U. Amaldi et al., Annu. Rev. Nucl. Sci. 26, 385 (1976).

11) U. Amaldi et al., Nucl. Phys. B145, 367 (1978).
K. Potter, ISR performance report ISR-ES/Kp/1p (1975).

12) K. Potter and S. Turner, IEEE Trans. Nucl. Sci. N522, 1589 (1975).

13) K. Brand and J.P. Gourber, CERN-ISR-BOM/77-3 (1977).

14) Private communication of K. Brand and J.P. Gourber.

15) Private communication of P. Bryant.

Table 1

Dimensions and positions of trigger hodoscopes

Trigger hodoscope	Inner radius (mm)	Outer radius (mm)	Distance from I.R. (mm)
H1	140	1300	2000
H2	140	1300	2000
H3	90	900	6400
H4	90	900	7700
TB	Elliptical R1 = 30 R2 = 78	$\gtrsim$ 300	8400

Table 2

Minimum and maximum angles (with respect to the beams) covered by trigger hodoscopes

Hodoscope or coincidence	θ_{min} (deg)	θ_{max} (deg)
CI	25.0	90.0
CO	31.6	90.0
H1	4.0	33.0
H2	4.0	33.0
H3	0.8	8.0
H4	0.7	6.7
TB	0.21	1.23
CI*CO	25.0	90.0
H1*H2	4.0	33.0
H3*H4	0.8	6.7
TB	0.3	1.23

Table 3

Dimensions of θ-bins and relative angles

Scintillator ring	H2θ				H4θ			
	Inner radius (mm)	Outer radius (mm)	Minimum angle (mrad)	Maximum angle (mrad)	Inner radius (mm)	Outer radius (mm)	Minimum angle (mrad)	Maximum angle (mrad)
1	140	220	70	110	90	110	11.7	14.3
2	220	320	110	159	110	130	14.3	16.9
3	320	430	159	212	130	150	16.9	19.5
4	430	560	212	273	150	170	19.5	22.1
5	560	700	273	337	170	190	22.1	24.7
6	700	840	337	398	190	220	24.7	28.6
7	840	990	398	460	220	260	28.6	33.8
8	990	1140	460	518	260	310	33.8	40.2
9	1140	1290	518	573	310	390	40.2	50.6
10					390	490	50.6	63.5
11					490	590	63.5	76.5
12					590	690	76.5	89.4
13					690	790	89.4	102.4
14					790	900	102.4	116.4

Table 4

Partial contributions of the various TOFs in typical runs at three different energies in the proton-proton reaction

TOF Cut in cascade[1)]	$\sqrt{s}$ = 23.5 GeV Contribution (%)	$\sqrt{s}$ = 44.7 GeV Contribution (%)	$\sqrt{s}$ = 62.7 GeV Contribution (%)
H_4-H_4	52.5	65.2	65.4
TB-H_4	1.9	3.9	4.4
H_4-TB	1.9	3.6	4.1
TB-TB	4.2	11.7	16.0
H_4-H_2	14.0	6.2	3.7
TB-H_2	0.5	0.4	0.3
H_2-H_4	14.0	5.9	3.8
H_2-TB	0.5	0.4	0.3
H_2-H_2	6.4	0.7	0.2
H_4-CO	3.0	1.7	1.6
TB-CO	0.1	0.1	0.1
H_2-CO	1.0	0.2	0.1
R_{meas}/R_{total}	98	95	93

Table 5

Elastic loss: calculation based on $(d\sigma/dt) \propto e^{-b|t|}$ and using proton data

$\sqrt{s}$ (GeV)	b $(GeV/c)^{-2}$	σ_{el} (mb)	$\Delta\sigma_{el}$ (mb)	η^{el}_{extr}
23.5	11.8 ± 1.18	6.77 ± 0.34	0.272 ± 0.03	0.007 ± 0.001
44.7	12.8 ± 1.28	7.2 ± 0.36	1.06 ± 0.11	0.027 ± 0.003
62.7	13.3 ± 1.33	7.57 ± 0.38	2.12 ± 0.21	0.053 ± 0.005

Table 6

Correction factors to compensate the loss of inelastic events at small angles

$\sqrt{s}$ (GeV)	η^{in}_{extr}
23.5	0.0027 ± 0.0005
44.7	0.0096 ± 0.002
62.7	0.0139 ± 0.003

Table 7

Summary of the errors affecting the determination of σ [$\sigma(\bar{p}p)$ is assumed equal to $\sigma(pp)$]

	$\Delta\sigma/\sigma$ (%)			Scale error
$\sqrt{s}$ (GeV)	23.5	44.7	62.7	$\Delta\sigma/\sigma$ (%)
Elastic loss	0.08	0.25	0.49	-
Inelastic loss	0.05	0.2	0.3	-
Background	-	-	-	0.1
Dead spaces	0.1	0.1	0.1	-
Randoms	$\lesssim$ 0.1	$\lesssim$ 0.1	$\lesssim$ 0.1	-
Luminosity	0.2	0.2	0.2	-
Total $\Delta\sigma/\sigma$ (%)	0.26	0.40	0.62	0.1

Figure captions

Fig. 1 : Total cross-section data for p, $\bar{p}$, π^+, π^-, K^+, K^- at laboratory momenta p_{lab} between 10 and 2000 GeV/c. Figure taken from Refs. 4 and 9.

Fig. 2 : Difference between $\sigma(\bar{p}p)$ and $\sigma(pp)$ as a function of laboratory momentum p_{lab} between 2 and 300 GeV/c. Data taken from Refs. 4 and 9.

Fig. 3 : Schematic layout of the experimental apparatus.

Fig. 4 : Schematic drawing of counter hodoscopes used for trigger definition.

Fig. 5 : Schematic drawing of hodoscope counters to measure the angular distribution.

Fig. 6 : View of the drift chamber central detector. 136 independent modules are held by 10 plexiglas containers (Ref. 8).

Fig. 7 : Typical raw TOF spectra measured in the PSB experiment at $\sqrt{s}$ = 22.6 GeV. (Ref. 1c).

Fig. 8 : $\bar{p}p$ topological cross-sections as a function of laboratory momentum p_{lab} between 2 and 100 GeV/c. Data taken from Refs. 4 and 9. The dashed curve is an extrapolation of zero-prong data in the ISR energy region.

Fig. 9 : Total elastic cross-section (upper side) and elastic slope b parameter for $\bar{p}p$ interaction (triangles) and pp interaction (open points) as a function of the laboratory momentum p_{lab} between 10 and 2000 GeV/c. Data taken from Ref. 10.

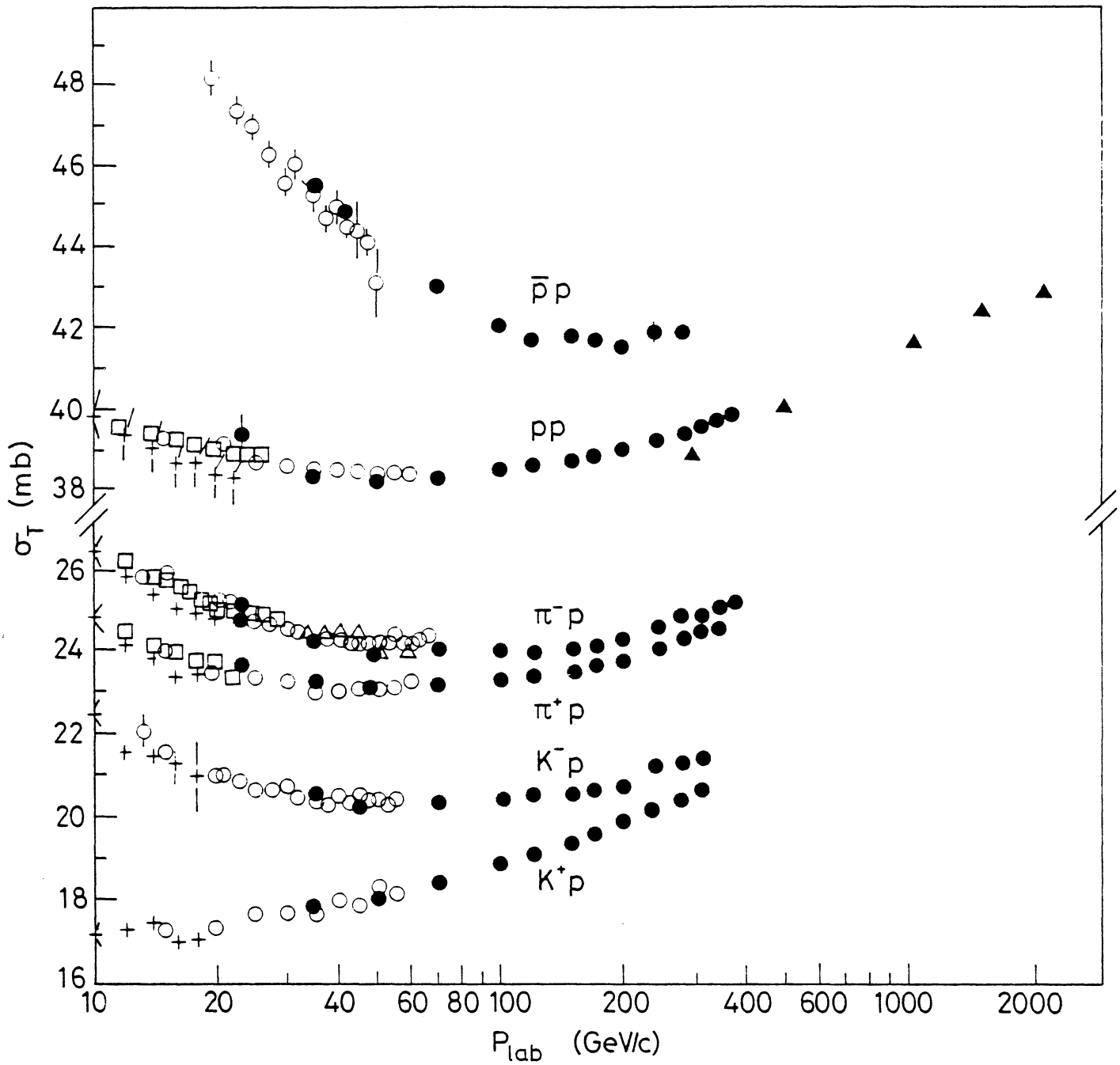
48
46
44
42
40
38
26
24
22
20
18
16
σ_T (mb)
$\bar{p}p$
pp
π^-p
π^+p
K^-p
K^+p
10
20
40
60
80
100
200
400
600
1000
2000
P_{lab} (GeV/c)

Fig. 1

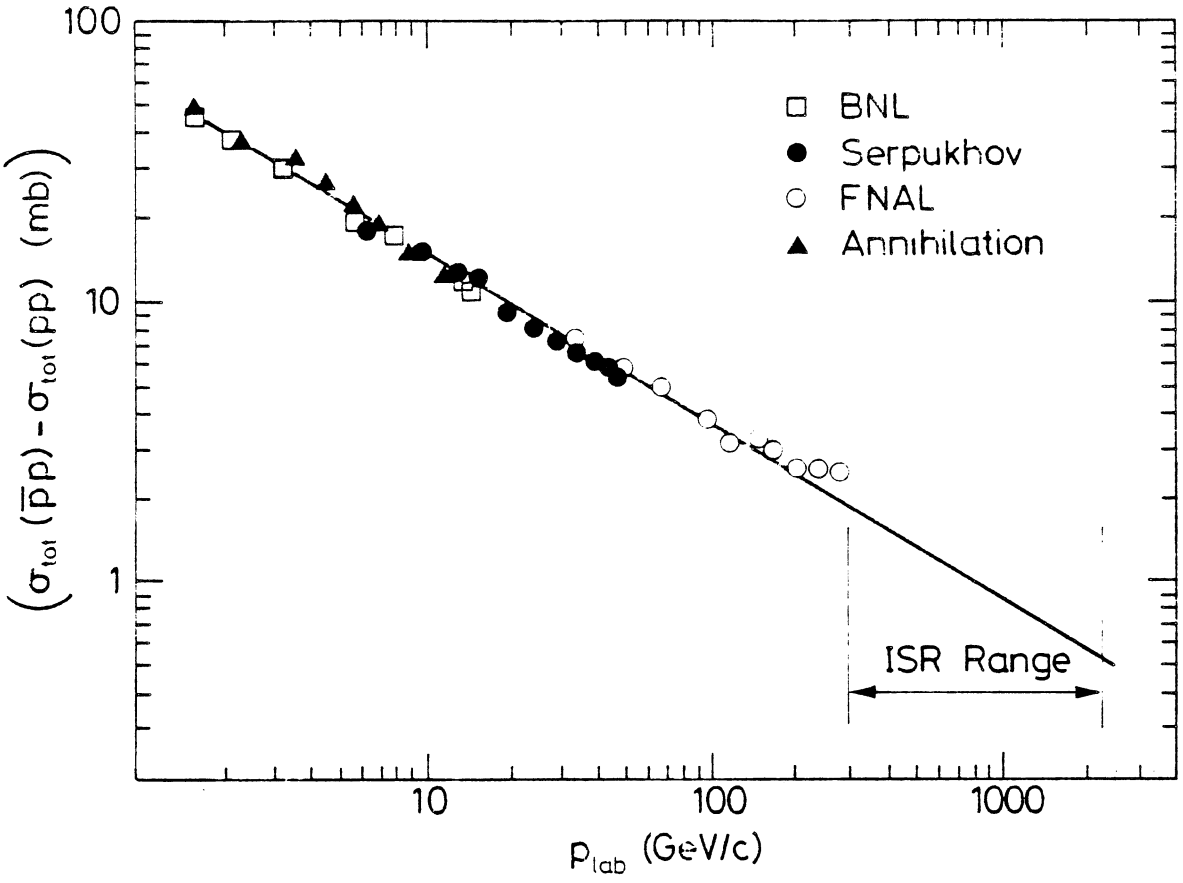
100
10
1
$(\sigma_{tot}(\bar{p}p) - \sigma_{tot}(pp))$ (mb)
BNL
Serpukhov
FNAL
Annihilation
ISR Range
10
100
1000
p_{lab} (GeV/c)

Fig. 2

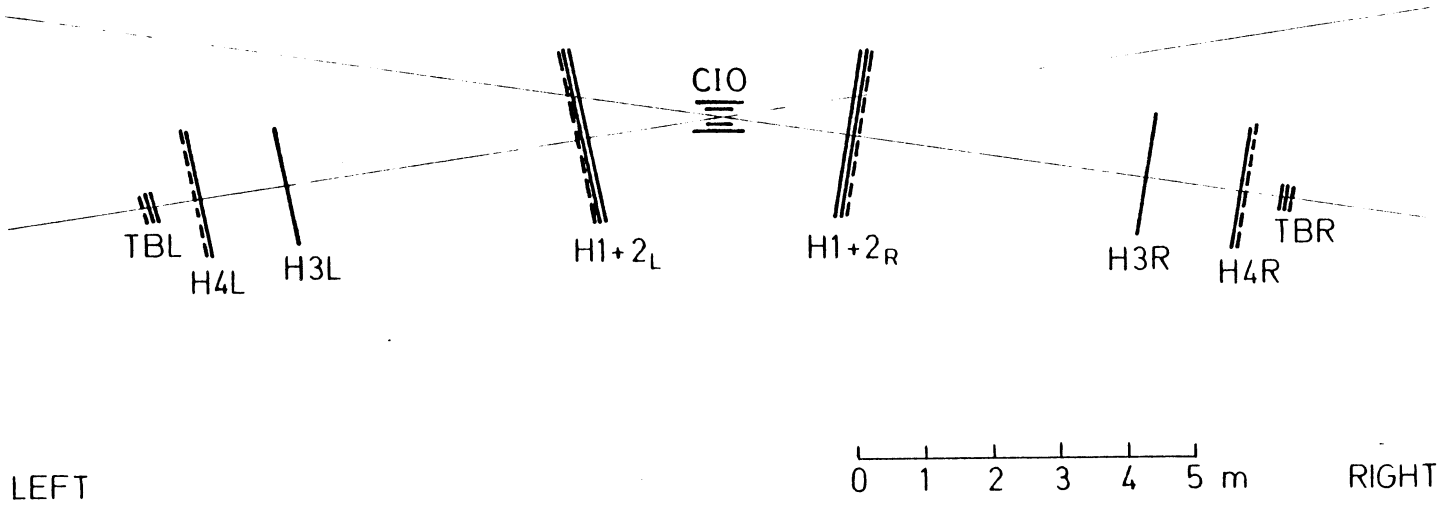

Fig. 3

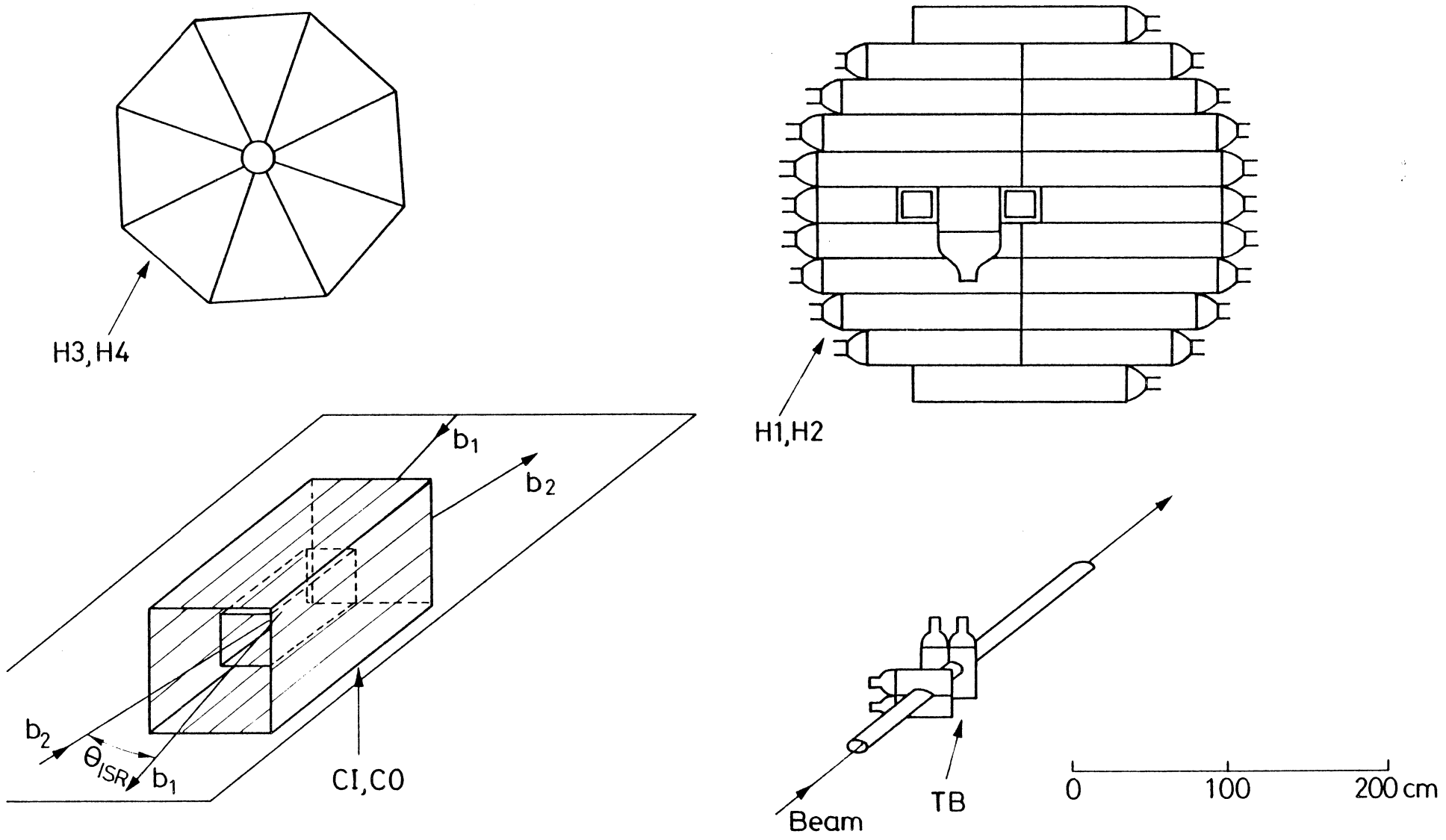

Fig. 4

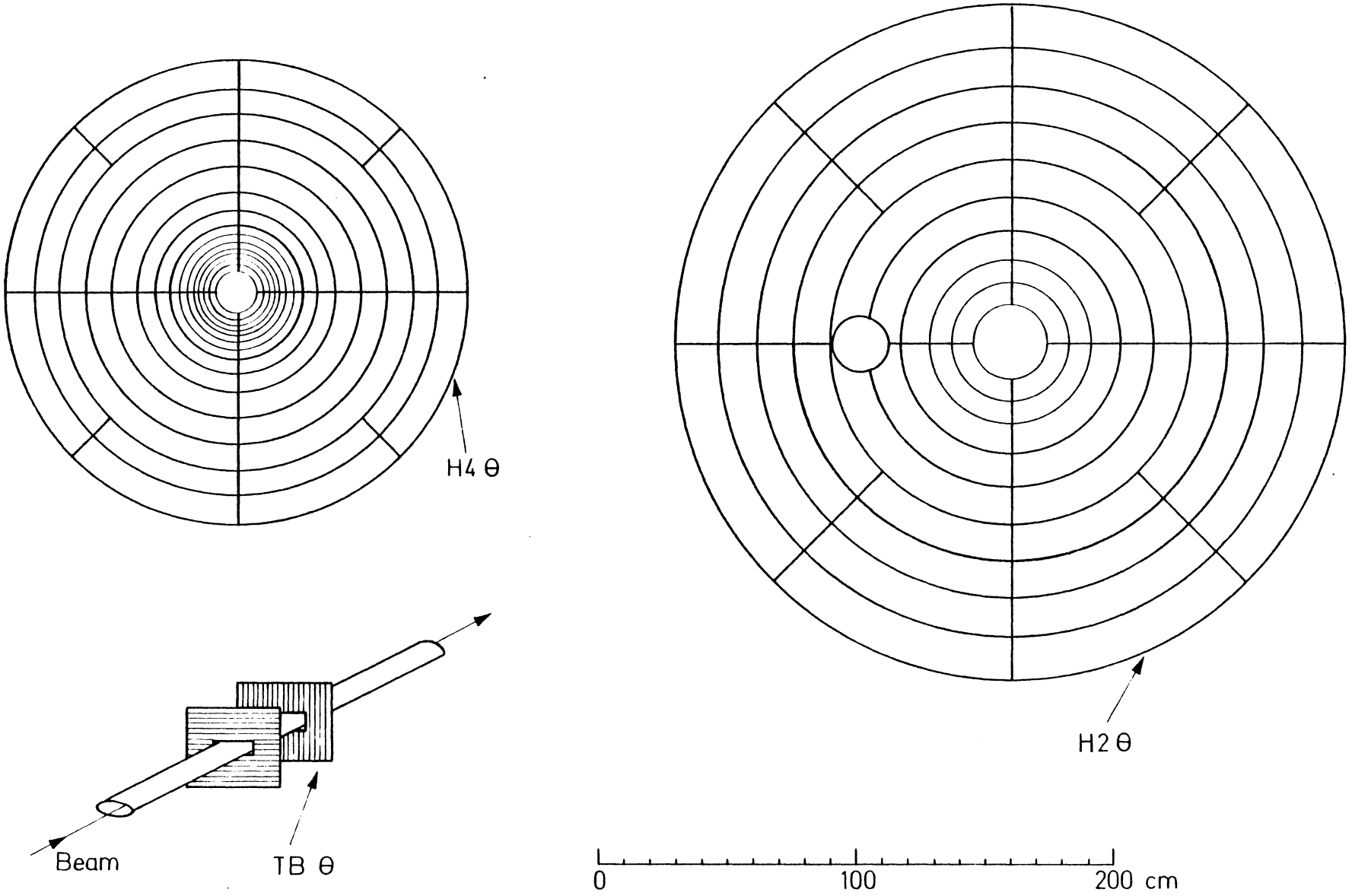

Fig. 5

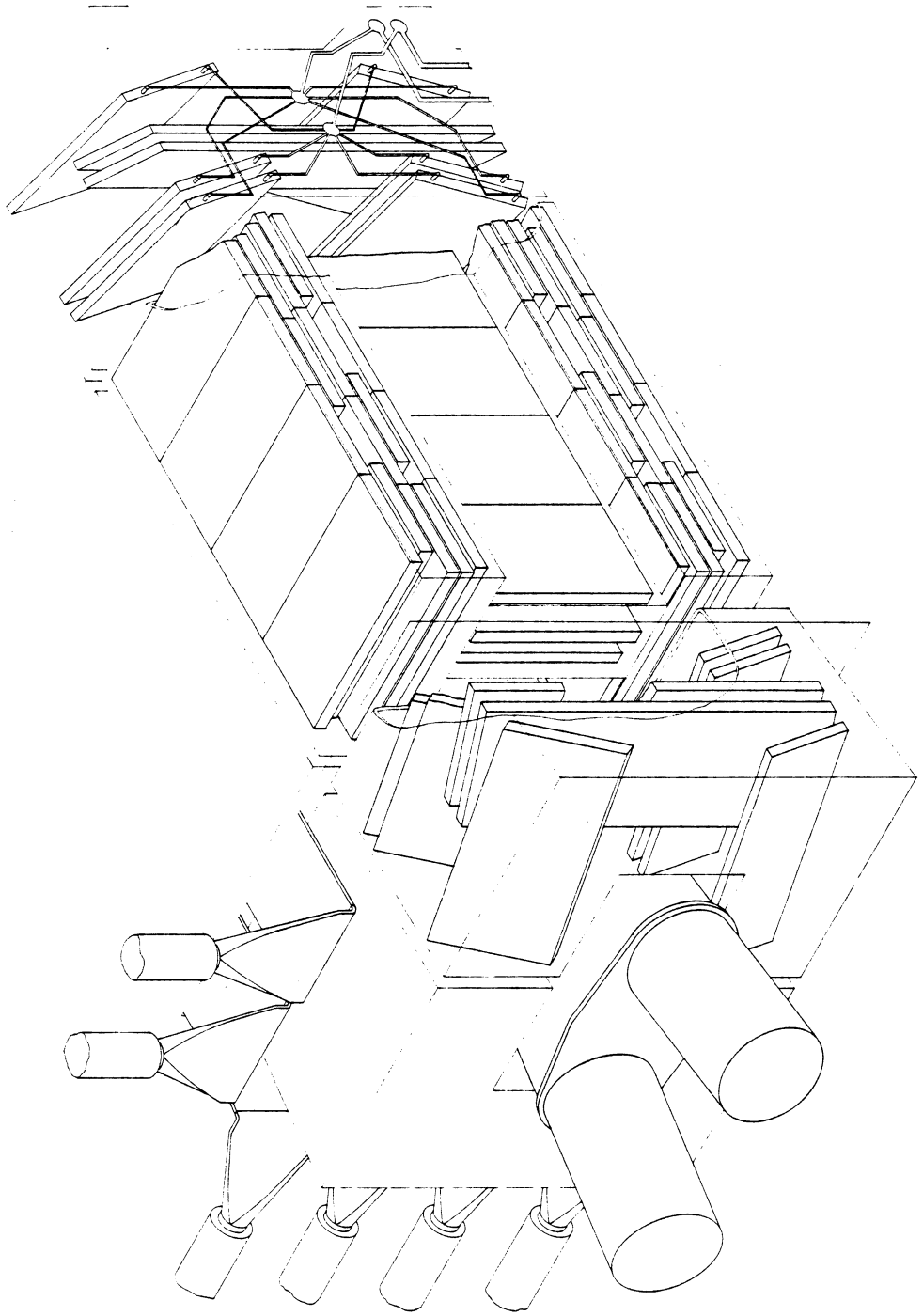

Fig. 6

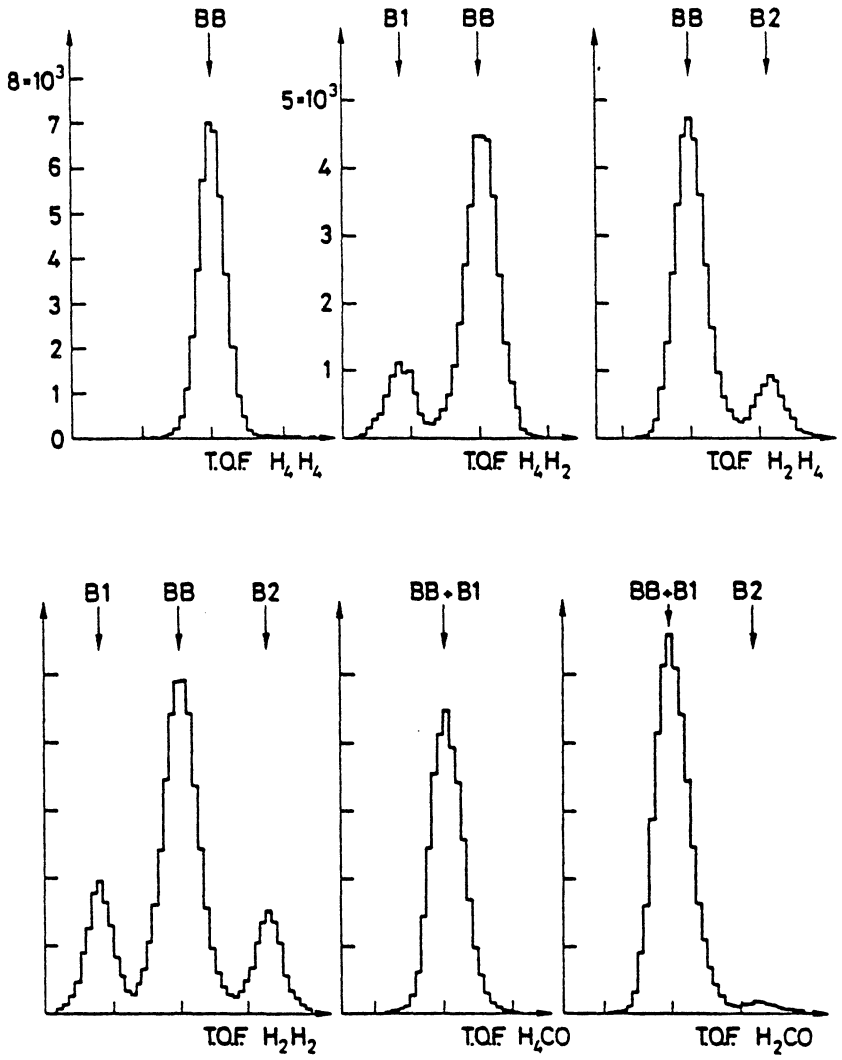
BB
B1
BB
BB
B2
8·10³
5·10³
T.O.F H₄H₄
T.O.F H₄H₂
T.O.F H₂H₄
B1
BB
B2
BB+B1
BB+B1
B2
T.O.F H₂H₂
T.O.F H₄CO
T.O.F H₂CO

Fig. 7

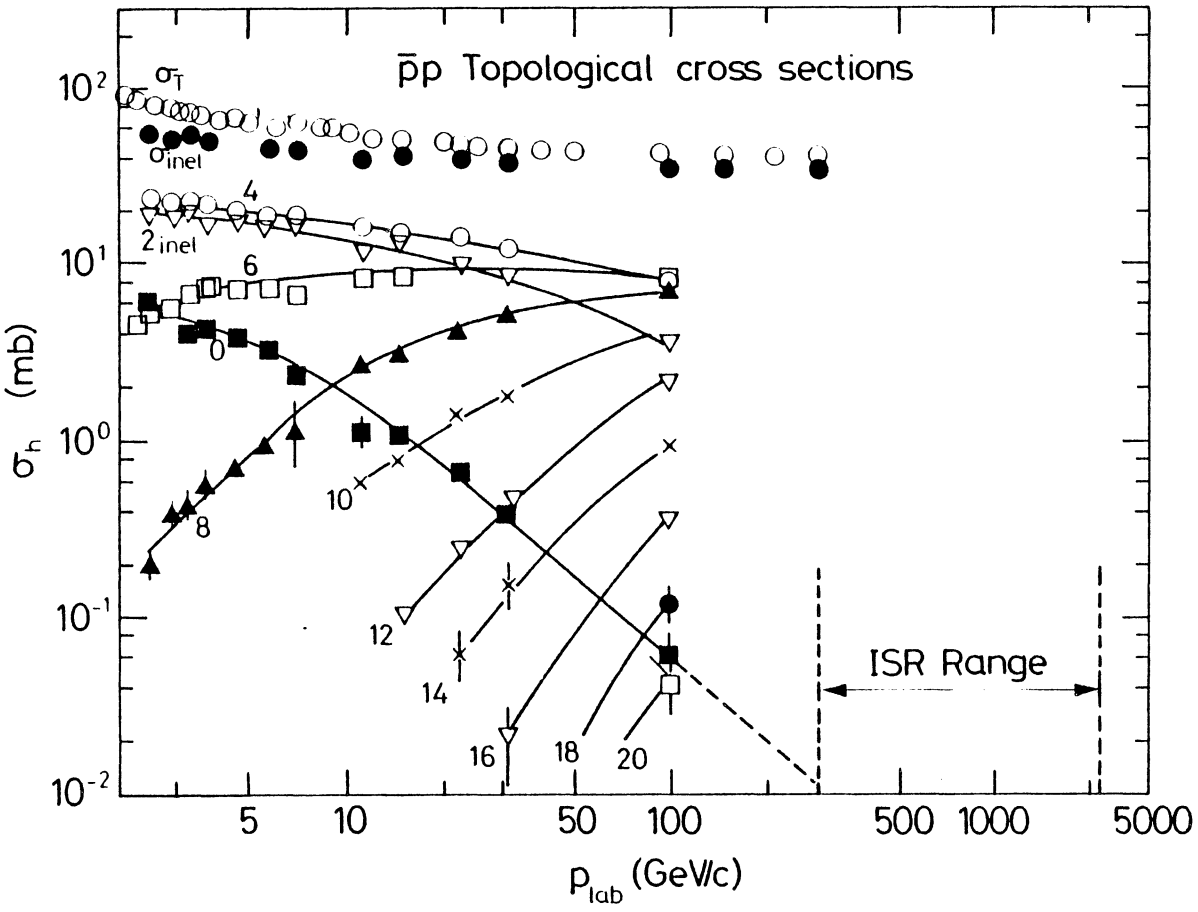
p̄p Topological cross sections
σ_T
σ_{inel}
2_{inel}
4
6
0
8
10
12
14
16
18
20
ISR Range
σ_n (mb)
10^2
10^1
10^0
10^{-1}
10^{-2}
5
10
50
100
500
1000
5000
p_{lab} (GeV/c)

Fig. 8

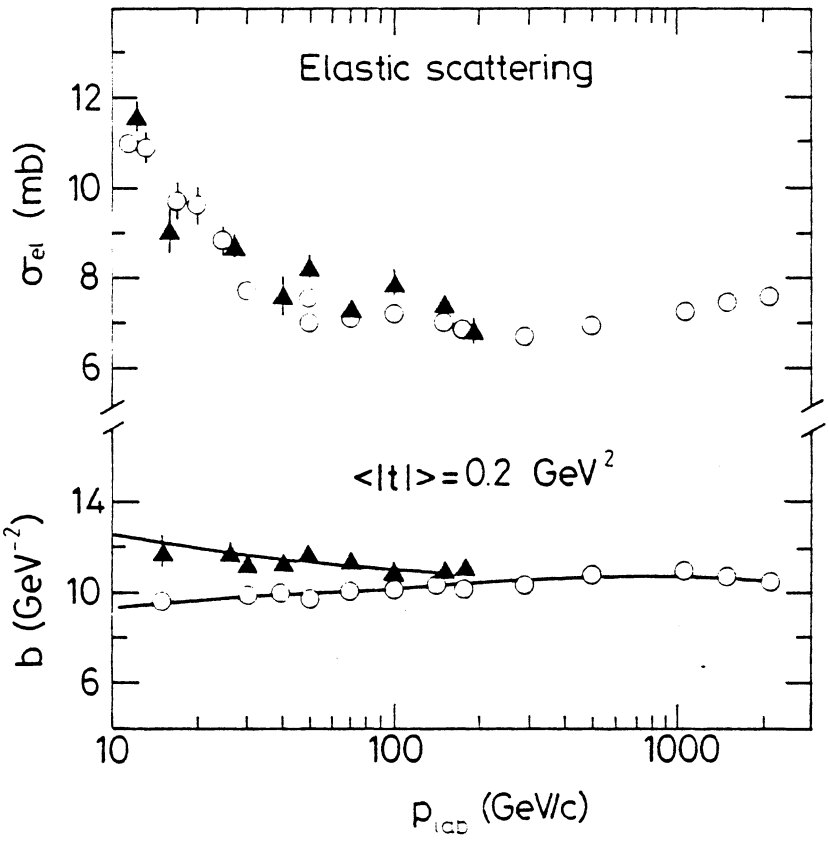
Elastic scattering
σ_{el} (mb)
12
10
8
6
<|t|>=0.2 GeV^2
b (GeV^{-2})
14
10
6
10
100
1000
p_{lab} (GeV/c)

Fig. 9